applied sciences

MDPI

Article

Homodyne Spectroscopy with Broadband Terahertz Power Detector Based on 90-nm Silicon CMOS Transistor

Kęstutis Ikamas [1,2,*], Dmytro B. But [3,4] and Alvydas Lisauskas [1,3,*]

1 Institute of Applied Electrodynamics and Telecommunications, Vilnius University, LT-10257 Vilnius, Lithuania
2 Research Group on Logistics and Defense Technology Management, General Jonas Žemaitis Military Academy of Lithuania, LT-10322 Vilnius, Lithuania
3 CENTERA Laboratory, Institute of High Pressure Physics PAS, 01-142 Warsaw, Poland; dbut@mail.unipress.waw.pl
4 CEZAMAT, Warsaw Technical University, 02-822 Warsaw, Poland
* Correspondence: kestutis.ikamas@ff.vu.lt (K.I.); alvydas.lisauskas@ff.vu.lt (A.L.)

Abstract: Over the last two decades, photomixer-based continuous wave systems developed into versatile and practical tools for terahertz (THz) spectroscopy. The high responsivity to the THz field amplitude of photomixer-based systems is predetermined by the homodyne detection principle that allows the system to have high sensitivity. Here, we show that the advantages of homodyne detection can be exploited with broadband power detectors combined with two photomixer sources. For this, we employ a THz detector based on a complementary metal-oxide-semiconductor field-effect transistor and a broadband bow-tie antenna (TeraFET). At 500 GHz and an effective noise bandwidth of 1 Hz, the response from one photomixer-based THz source resulted in an about 43 dB signal-to-noise ratio (SNR). We demonstrate that by employing a homodyne detection system by overlaying the radiation from two photomixers, the SNR can reach up to 70 dB at the same frequency with an integration time 100 ms. The improvement in SNR and the spectroscopic evidence for water vapor lines demonstrated up to 2.2 THz allow us to conclude that these detectors can be successfully used in practical continuous wave THz spectrometry systems.

Keywords: THz power detector; terahertz detector; broadband antenna; field-effect transistor; homodyne detection; terahertz spectroscopy

Citation: Ikamas, K.; But, D.B.; Lisauskas, A. Homodyne Spectroscopy with Broadband Terahertz Power Detector Based on 90-nm Silicon CMOS Transistor. *Appl. Sci.* **2021**, *11*, 412. https://doi.org/10.3390/app11010412

Received: 30 November 2020
Accepted: 29 December 2020
Published: 4 January 2021

1. Introduction

In recent decades, the terahertz band of electromagnetic waves (THz) has received much attention. The peculiarities of interaction of electromagnetic radiation with many materials at this frequency band give THz an important place in spectroscopy, as well as imaging applications, e.g., for the investigation of molecular crystals and organic molecules [1], for the detection of the concealed weapons or chemical recognition of explosives at airports [2,3], for the detection of drugs and malignant tumors in medicine [4], as well as for quality control systems in industry [5]. THz spectroscopy is also used to study many-body quantum kinetics [6], to discover the cosmic microwave background radiation and interstellar cloud in astronomy [7], and for art conservation [8]. Therefore, by now, there are many reports related to the application of THz technologies in various fields of science: physics, chemistry, biology, medicine, and telecommunication [9,10].

Over the last two decades, the photomixer-based continuous wave systems developed into versatile and practical THz spectroscopy tools [11]. The high sensitivity of photomixer-based systems comes from their sensitivity to the THz field amplitude, which is predetermined by the inherent homodyne detection principle [12]. Moreover, this technique allows estimating frequency-dependent changes in the optical path, allowing for simultaneous assessment of an absorption and a refractive index, i.e., a complex dielectric function.

Recently the development of photonic THz systems took a path that combines photo-switch-based generation and a fast power detector (zero-biased Schottky diode) [13]. This solution became attractive for applications that prefer fast response, and the spectral discrimination was not of primary interest. Whereas commercially offered systems employ zero-bias Schottky diode detectors, there were reports that demonstrated that TeraFETs could also be used in conjunction with time-domain photonic systems [14,15]. Furthermore, CMOS TeraFETs have been reported to be effectively applied as detectors for photomixer-generated THz frequency combs [16].

The advantages of homodyne detection can also be exploited by utilizing broadband power THz detectors and a photimixer-based THz generation scheme. In the beginning, Schottky diodes were demonstrated as candidates for mixing two THz waves [17]. Recently, a diode of an asymmetrically-shaped bow-tie geometrical form was used for homodyne-based imaging [18]. Reported state-of-the-art performance [19–21] values prove that field-effect transistors (FET) are becoming strong competitors to other established THz detection technologies. The technological handling, temperature stability, and large-area high-volume integration of FETs are, however, much easier to use, because unlike Schottky diodes, they are part of the mature standard processing technology of microelectronics, which is now projected for novel THz photonic use.

Successful homodyne detection at a single frequency in the THz range with FET was demonstrated several times [22–24]. Recently, a homodyne-based phase-sensitive terahertz spectrometer concept that utilizes FET as a detector was proposed [25]. Here, we present experimental evidence supporting this theory. We employ a THz detector based on 90 nm Si CMOS FET and broadband bow-tie antenna (also called TeraFET).

2. Si CMOS Detector

The planar antenna-coupled THz detector based on Si CMOS FET was used for experiments. The TeraFET employs a single-transistor layout based on the n-MOS transistor with an ultra-low threshold voltage of 445 mV, where the channel length is 100 nm and the width is 1 µm. The device was fabricated by TSMC (Taiwan, a foundry service provided by Europractice) using a 90 nm technological node. The TeraFET design was optimized using an in-house developed physics-based circuit model [20,21].

The antenna is implemented in the metal-dielectric stack of the CMOS's back-end. Each antenna leaf consists of two almost identical shapes, arranged in two metal layers (see Figure 1b). The circuit of connections between the antenna leaves and transistor contacts ensures asymmetric power coupling into the channel from the source side only, which is an essential condition of plasma-wave rectification [26–29]. Additionally, it ensures the necessary electrical isolation between the gate terminal for applying DC bias and the readout of the rectified signal from the drain terminal. More details on the design can be found in [21]. Antenna *EM* analysis results have shown that the bigger part of the *EM* energy is emitted into the semiconductor substrate side rather than into the air. Therefore, an additional Si substrate lens is required for efficient coupling between an antenna and THz radiation, which is directed from the substrate side.

For the characterizations of detector response, we employed a tunable multiplier-based source fabricated by Virginia Diodes Inc. (VDI) as well as photomixer sources fabricated by Toptica GmbH (more details on the measurement technique can be found in [21,30]). The VDI source can be tuned over a frequency range from 500 to 750 GHz, and Toptica's—from 50 GHz to 2.2 THz. Our experimental setup for homodyne detection includes two InGaAs photodiodes with a bow-tie photoconductive antenna (labeled TX). The photomixers include hyperhemispherical Si lenses and have slight differences in output characteristics. More information on specific properties of TX modules can be found in [31]. For the calibration of available THz power, we used a large aperture detector from Thomas Keating Ltd. In addition, we performed comparisons of detector broadband performance with a Golay cell detector purchased from Tydex Optics Inc. and a calibrated pyroelectric detector. The last one was manufactured by SLT Sensor GmbH [32], and it has a 20 mm

aperture and 42.3 V/W sensitivity (its calibration was provided in combination with a preamplifier by the manufacturer at 1.4 THz).

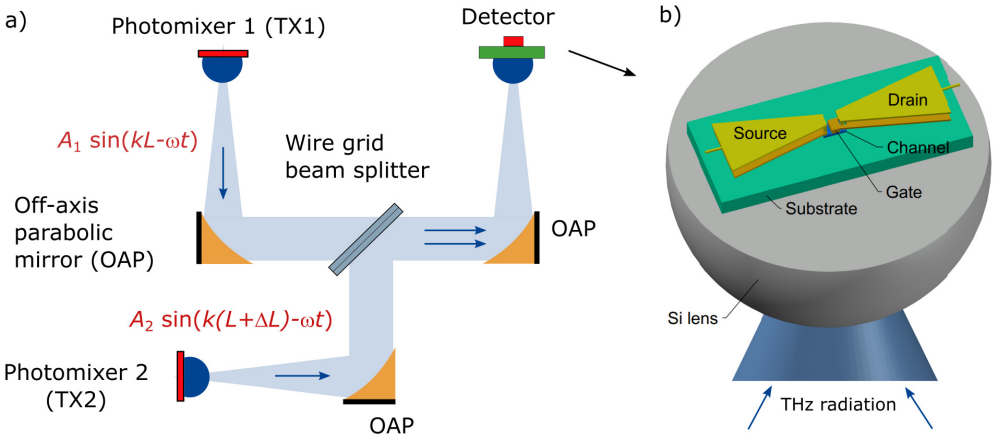

Figure 1. (**a**) The THz homodyne measurements' optical setup. (**b**) Simplified schematic image of the THz detector. The dimensions of the antenna metallization (yellow) and of the Si lens (grey) are not to scale in order to demonstrate the device structure clearly.

Figure 2a provides the detector's optical voltage responsivity $\Re_V$ (V/W) as a function of the gate voltage V_g. The responsivity is calculated from the measured peak-to-peak value of voltage response V_{det} and the power in the beam:

$$\Re_V = \frac{V_{det}}{P_{THz}}, \tag{1}$$

where P_{THz} is a peak-to-peak value of an incident THz power, which in our measurements with the VDI multiplier source was 10 µW at 609 GHz. For direct power response measurements, we used an 880 Hz chopping frequency. The maximal modulation frequency of TeraFET can reach as high as a typical cut-off frequency $f_T \approx 100$ GHz; however, the speed of response of the practical system is limited by the read-out circuitry, which for our devices was about 4 MHz.

The knowledge of optical responsivity, as well as the resistance of the channel with the concomitant spectral density of voltage fluctuations, enables estimation of the NEP for these detectors, which is presented in Figure 2a. The NEP of the detector can be derived as:

$$NEP = \frac{\sqrt{4k_B T R_{DC} \Delta f}}{\Re_V}, \tag{2}$$

where k_B is the Boltzmann's constant, T is the room temperature, R_{DC} is the DC resistance of the transistor's channel and Δf is the equivalent noise bandwidth. The dimension of such a defined quantity is given in W/$\sqrt{\text{Hz}}$. Later in Section 4, we will present experimental noise measurements that validate the applicability of Equation (2).

The maximum responsivity and NEP values appear at different gate voltages (compare both curves in Figure 2a). This is due to the nonlinear dependency of the DC drain-source resistance R_{DC} on the gate voltage. The maximum voltage response, and corresponding responsivity, were at the gate voltage bias 180 mV, and the minimum NEP was at 475 mV. In the following experiments, the detector was biased with the gate voltage of 475 mV, which represents the device's working regime with the best NEP values.

In the system with a VDI multiplier as a source, the TeraFET exhibited an optical voltage responsivity of 193 V/W (current responsivity of 38 mA/W) and a minimum optical NEP as low as 47 pW/$\sqrt{\text{Hz}}$ at 609 GHz. It should be pointed out that the presented values are the optical ones for the detector module, i.e., in the calculation, we used the total available THz beam power at the position of the detector (measured after all OAP

mirrors, attenuators, and other optical elements). Hence, the optical losses introduced by the detector module itself, such as in a silicon lens or radiation coupling to the integrated antenna, are not deducted.

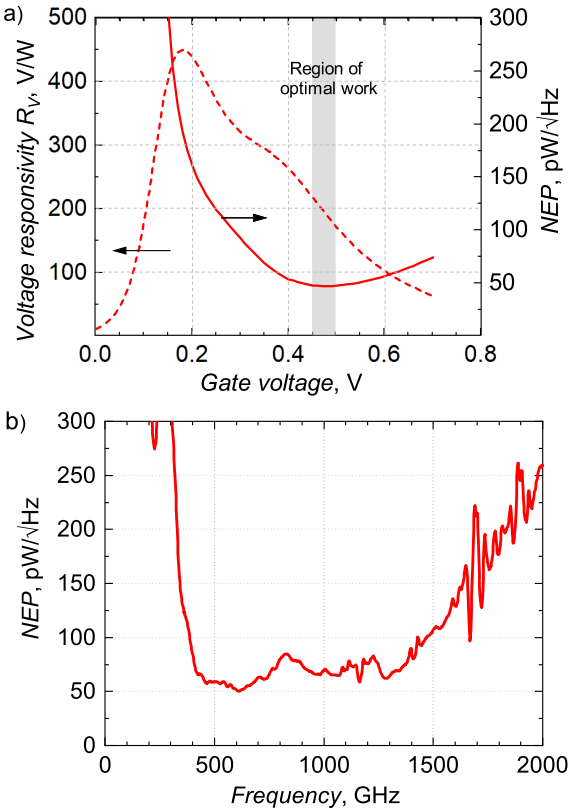

Figure 2. (**a**) The measured optical voltage responsivity $\Re_V$ (dashed curve, left axis) and optical NEP (solid curve, right axis) of the detector at 609 GHz as a gate voltage function. The VDI source was used for measurements. (**b**) The measured optical NEP dependency on a frequency of the photomixer source used in the homodyne experiment.

We also measured our detector's broadband performance in the Toptica system, where an original photomixer detector was replaced with the TeraFET (Figure 2b). The used sample exhibited a nearly flat frequency response characteristic from 0.4 up to 1.4 THz. The achieved minimum optical NEP was as low as 50 pW/$\sqrt{\text{Hz}}$ at 0.6 THz and 81 pW/$\sqrt{\text{Hz}}$ at 1.4 THz. The slightly worse detector characteristics in the Toptica system can be explained by a different beam profile and optical setup differences.

3. Experiment Setup for Homodyne Detection

For the characterization of the TeraFET's homodyne response in a broad frequency range from 0.1 up to 2.2 THz, we used two similar photomixer-based THz sources from the Toptica system in a homodyne scheme (TX1 and TX2, see Figure 1a) with a modulation frequency of 7.9 kHz. For the collimation and focusing of two THz beams onto the test detector, we constructed an imaging system with a two-inch diameter and four-inch effective focal length off-axis parabolic mirrors and a wire grid beamsplitter. The THz radiation is incident on the antenna from the detector's bottom through a hyper-hemispherical silicon lens and a reduced, 280 µm thick p-doped Si substrate of the chip. The lens has 12 mm diameter and 7.2 mm height with an additional 440 µm thick substrate. The THz beams are modulated electrically with a built-in function generator enabling to employ the lock-in amplifier.

Similarly, as it is used in a commercial photomixer-based system, we have not performed any additional effort regarding phase stabilization. We relied on a built-in

laser control, which was developed by Toptica GmbH, providing good measurement-to-measurement reproducibility of laser emission frequencies when the lasers are temperature-stabilized; additionally, the external conditions did not vary, thus maintaining the same spatial delay. In order to test the similarity of THz bias-modulated photomixers, we measured the frequency-dependent responses of the detector on both setup arms. The characterization results are presented in Figure 3a. Both sources provide a maximum THz output power at 100 GHz and fade out nearly exponentially with frequency. In a broad range, photomixers exhibited similar power levels except for a narrow band (120–350 GHz) where the difference reached 50%. The difference in the response values for TX1 and TX2 is related to the loss on a wire grid combiner and the differences in the individual sources' performances.

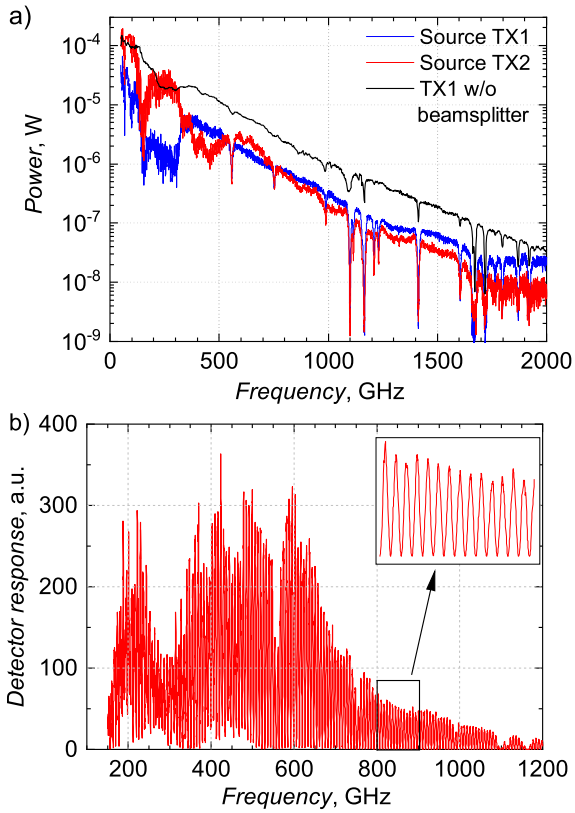

Figure 3. (**a**) Power of the THz sources in the homodyne experiment setup (marked as TX1, blue line, and TX2, red line). The measurement was provided using the same TerFET detector at the gate voltage of 475 mV. The reference measurement of the original Toptica system's power with only one source TX1 is also presented for comparison purposes (black line). It was recorded with the pyroelectric detector. (**b**) Measured homodyne signal of TeraFET, which was biased at the same gate voltage. The magnification shows oscillations.

The theory predicts that TeraFETs, when excited with low powers, behave as linear power detectors. The response linearity is maintained in different material systems [33] as well as for different biasing regimes [15,34]. The TeraFET's voltage signal is proportional to the THz beam power and can be expressed using (1) as:

$$V_{\mathrm{det}} = \Re_{\mathrm{V}} \cdot P_{\mathrm{THz}} \propto \Re_{\mathrm{V}} \cdot V_{\mathrm{THz}}^2, \tag{3}$$

where the radiation power P_{THz} is proportional to the squared excitation amplitude V_{THz}. The difficulty of detecting a weak signal of sub-millimeter radiation can be reduced using a well-known homodyne technique. In a homodyne detection scheme, the detector is excited with two superimposed beams oscillating with the same angular frequency ω but differentiating in phase and/or amplitude (see Figure 1a). The phase can be introduced in

the form of a difference in beam paths ΔL. The voltage signal of TeraFET can be defined by the following formula:

$$V_{\text{det}}(\Delta L) \propto \frac{1}{2\pi/\omega} \int_0^{2\pi/\omega} [A_1 \sin(kL - \omega t) + A_2 \sin(k(L + \Delta L) - \omega t)]^2 dt. \quad (4)$$

where A_1 and A_2 are the amplitudes of the first and second beams, respectively, and k is a wavenumber, which is related to a wavelength λ or a frequency as $k = 2\pi/\lambda = \omega/c$. The equation can be reduced to the following form:

$$V_{\text{det}}(\Delta L) \propto \frac{A_1^2 + A_2^2}{2} + A_1 A_2 \cos(k\Delta L). \quad (5)$$

The first term is the average power. By changing frequency, the $\omega/c\Delta L$ varies from 0 to 2π, and the envelope of the detector's response dependency on an excitation frequency $V_{\text{det}}(\omega)$ has a cosine form (so-called fringe spectrum, see the magnification in Figure 3b). We can also change a phase with mechanical XY stages or opaque materials, such as a paper Si attenuator.

The detector in the homodyne detection setup exhibits the same noise as for direct detection; however, it provides the difference signal in addition, which is not influenced by the noise of the THz source. The main advantage of homodyne detection is the ability to detect weaker excitation compared to a direct detection scheme.

4. Results and Discussions

The TeraFET response on the homodyne excitation at different gate bias voltages is presented in Figure 4a. For low gate voltages (below the threshold point at 445 mV), the voltage response is higher; however a signal-to-noise ratio (SNR) is lower due to an increase in noise. The SNR is defined as the ratio between the rms amplitude of the measured signal and the standard deviation of noise values. The best SNR for the investigated detector was obtained at a gate voltage bias of 475 mV. The graph also shows measured detector noise levels (dashed lines) obtained from the recorded statistics (standard deviation) of the response while blocking THz beams with an opaque metallic plate placed in front of the detector. These data allow calculating the dynamic range of device sensitivity as well as comparing with the theoretically expected thermal Johnson–Nyquist noise for the unbiased TeraFET's channel [35,36]. The theoretical noise voltage can be calculated using the simple equation $V_{\text{noise}} = \sqrt{4k_B T R_{\text{DC}} \Delta f}$, where the equivalent noise bandwidth Δf in our case was equal to 1.25 Hz (for 100 ms integration time). V_{noise} is shown in Figure 4a with hollow symbols. The measured detector noise levels correspond well to the theoretically expected thermal noise limit, which indicates good noise suppression techniques (such as shielding or removing ground loops) implemented in our setup, and validates the NEP results presented in Figure 2.

However, even when the detector noise was mainly of thermal origin, response curves showed similar additional signals at high frequencies (above 1.7 THz). The origin of this signal is not yet clearly understood. It can be either below 100 GHz as the result of beating between laser Fabry–Perrot modes or very broadband IR radiation from the local heating of the photomixer. There were several recent reports that the TeraFET detector could act as a detector of passive radiation [37,38]. The same is expected from Schottky-diode detectors.

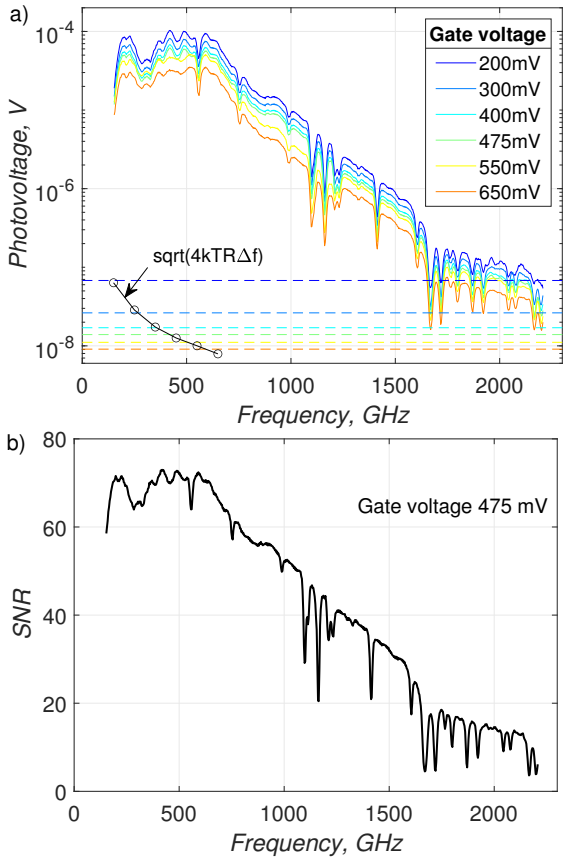

Figure 4. (**a**) Comparison of homodyne system signals for different gate biases. The corresponding noise levels for each bias are marked with dashed lines. The black hollow dots are the calculated noise level of the detector (thermal noise). (**b**) The frequency-dependent signal-to-noise ratio of the THz detector at the gate voltage of 475 mV.

Figure 4b shows the dynamic range of the measured response's dependency on the frequency for the gate voltage bias of 475 mV. The dynamic range reached a signal-to-noise ratio (SNR) of over 70 dB at 500 GHz and 100 ms integration time. The commercial homodyne system based on the same photomixer emitter and additional photomixer receiver can reach an SNR of ca. 83 dB, as declared by the manufacturer in the specification and confirmed by our independent tests. In our experimental work with one photomixer-based THz source [21], TereFET's SNR was 43 dB at 500 GHz and 100 ms. However, the commercial system uses a setup with four two-inches mirrors, which allows having the smallest losses in the optical path. The investigated system is based on a wire grid polarizer that divides each beam and total power in two. The second optical branch after the polarizer can be used in the future, for example, for additional reflection measurements.

The observed improvement in SNR of the TeraFET using the homodyne detection technique compared to the direct one could represent clearly seen water vapor lines [39] for frequencies over 2 THz, as shown in Figure 4b in comparison to Figure 3a. This allows us to conclude that these detectors can find practical application in continuous-wave THz spectrometry systems. Adding the second detector to the same system will allow to simultaneously record transmission and reflection amplitudes as well as propagation delay times, and therefore to measure complex dielectric properties as with heterodyne-based vector network analyzers. TeraFETs have an advantage in comparison with other uncooled semiconductor THz power detectors in that they can be manufactured using mature commercial microchip mass-production technologies and hence can be realized as large-area matrices.

5. Conclusions

We demonstrated an effective homodyne detection system by employing a THz FET detector. The homodyne detection technique allows improving the SNR by up to 70 dB at the same frequency with a 100 ms integration time, which is more than 25 dB better than a direct detection system with the same components. The observed improvement in SNR using the homodyne technique with the TeraFET detector allows us to conclude that THz FET detectors can be successfully applied to continuous-wave THz spectrometry systems. Adding a second TeraFET detector to the same setup will allow us to simultaneously record transmission and reflection amplitudes as well as signal propagation delay times. Therefore, it opens the possibility to measure the complex dielectric properties of materials in the same way as with heterodyne-based vector network analyzers.

Author Contributions: Conceptualization, A.L.; methodology, A.L.; software, K.I. and D.B.B.; formal analysis, K.I.; investigation, K.I. and D.B.B.; data curation, K.I.; writing—original draft preparation, K.I.; writing—review and editing, D.B.B. and A.L.; supervision, A.L.; funding acquisition, A.L. All authors have read and agreed to the published version of the manuscript.

Funding: This research was partially supported by the "International Research Agendas" program of the Foundation for Polish Science co-financed by the EU under the European Regional Development Fund (No. MAB/2018/9) for CENTERA.

Institutional Review Board Statement: Not applicable.

Informed Consent Statement: Not applicable.

Data Availability Statement: Not applicable.

Acknowledgments: The authors would like to thank the THz research group from the University of Frankfurt, led by Roskos, for long-standing fruitful cooperation in developing THz detectors. The detector employed here was created within the scientific cooperation between the Frankfurt and Vilnius Universities' groups on a cost-sharing basis.

Conflicts of Interest: The authors declare no conflict of interest. The funders had no role in the design of the study; in the collection, analyses, or interpretation of data; in the writing of the manuscript; or in the decision to publish the results.

Abbreviations

The following abbreviations are used in this manuscript:

THz	terahertz
FET	field-effect transistor
TeraFET	field-effect transistor with integrated antennas for THz detection
CMOS	complementary metal-oxide-semiconductor
Si	silicon
NEP	noise-equivalent power
SNR	signal-to-noise ratio

References

1. Sasaki, T.; Sakamoto, T.; Otsuka, M. Detection of Impurities in Organic Crystals by High-Accuracy Terahertz Absorption Spectroscopy. *Anal. Chem.* **2018**, *90*, 1677–1682. [CrossRef] [PubMed]
2. Palka, N.; Szala, M.; Czerwinska, E. Characterization of prospective explosive materials using terahertz time-domain spectroscopy. *Appl. Opt.* **2016**, *55*, 4575–4583. [CrossRef] [PubMed]
3. Federici, J.; Schulkin, B.; Huang, F.; Gary, D.; Barat, R.; Oliveira, F.; Zimdars, D. THz imaging and sensing for security applications—Explosives, weapons and drugs. *Semicond. Sci. Technol.* **2005**, *20*, S266–S280. [CrossRef]
4. Danciu, M.; Alexa-Stratulat, T.; Stefanescu, C.; Dodi, G.; Tamba, B.I.; Mihai, C.T.; Stanciu, G.D.; Luca, A.; Spiridon, I.A.; Ungureanu, L.B.; et al. Terahertz Spectroscopy and Imaging: A Cutting-Edge Method for Diagnosing Digestive Cancers. *Materials* **2019**, *12*, 1519. [CrossRef] [PubMed]
5. Bauer, M.; Döring, M.; Degenhardt, U.; Friederich, F. Terahertz Inspection of the Joining Quality of Industrial Silicon Carbide Ceramics. In Proceedings of the 2019 44th International Conference on Infrared, Millimeter, and Terahertz Waves (IRMMW-THz), Paris, France, 1–6 September 2019; pp. 1–2.

6. Lloyd-Hughes, J. Terahertz spectroscopy of quantum 2D electron systems. *J. Phys. D Appl. Phys.* **2014**, *47*, 374006. [CrossRef]
7. Richter, H.; Wienold, M.; Schrottke, L.; Biermann, K.; Grahn, H.T.; Hübers, H.W. 4.7-THz Local Oscillator for the GREAT Heterodyne Spectrometer on SOFIA. *IEEE Trans. Terahertz Sci. Technol.* **2015**, *5*, 539–545. [CrossRef]
8. Jackson, J.B.; Bowen, J.; Walker, G.; Labaune, J.; Mourou, G.; Menu, M.; Fukunaga, K. A Survey of Terahertz Applications in Cultural Heritage Conservation Science. *IEEE Trans. Terahertz Sci. Technol.* **2011**, *1*, 220–231. [CrossRef]
9. Tonouchi, M. Cutting-edge terahertz technology. *Nat. Photonics* **2007**, *1*, 97–105. [CrossRef]
10. Nagatsuma, T. Terahertz technologies: Present and future. *IEICE Electron. Express* **2011**, *8*, 1127–1142. [CrossRef]
11. Jepsen, P.; Cooke, D.; Koch, M. Terahertz spectroscopy and imaging—Modern techniques and applications. *Laser Photonics Rev.* **2011**, *5*, 124–166. [CrossRef]
12. Deninger, A.J.; Roggenbuck, A.; Schindler, S.; Preu, S. 2.75 THz tuning with a triple-DFB laser system at 1550 nm and InGaAs photomixers. *J. Infrared Millim. Terahertz Waves* **2015**, *36*, 269–277. [CrossRef]
13. Rettich, F.; Vieweg, N.; Cojocari, O.; Deninger, A. Field Intensity Detection of Individual Terahertz Pulses at 80 MHz Repetition Rate. *J. Infrared Millim. Terahertz Waves* **2015**, *36*, 607–612. [CrossRef]
14. Ikamas, K.; Lisauskas, A.; Massabeau, S.; Bauer, M.; Burakevič, M.; Vyšniauskas, J.; Čibiraitė, D.; Krozer, V.; Rämer, A.; Shevchenko, S.; et al. Sub-Picosecond Pulsed THz FET Detector Characterization in Plasmonic Detection Regime Based on Autocorrelation Technique. *Semicond. Sci. Technol.* **2018**, *33*, 124013. [CrossRef]
15. Ikamas, K.; Nevinskas, I.; Krotkus, A.; Lisauskas, A. Silicon Field Effect Transistor as the Nonlinear Detector for Terahertz Autocorellators. *Sensors* **2018**, *18*, 3735. [CrossRef]
16. Martín-Mateos, P.; Čibiraitė-Lukenskienė, D.; Barreiro, R.; de Dios, C.; Lisauskas, A.; Krozer, V.; Acedo, P. Hyperspectral Terahertz Imaging with Electro-Optic Dual Combs and a FET-Based Detector. *Sci. Rep.* **2020**, *10*, 14429. [CrossRef]
17. Schoenherr, D.; Cojocari, O.; Sydlo, C.; Goebel, T.; Feiginov, M.; Hartnagel, H.L.; Meissner, P. Optical mixing in THz Schottky diodes. In Proceedings of the 2008 33rd International Conference on Infrared, Millimeter and Terahertz Waves, Pasadena, CA, USA, 15–19 September 2008; pp. 1–2.
18. Jokubauskis, D.; Minkevičius, L.; Seliuta, D.; Kašalynas, I.; Valušis, G. Terahertz Homodyne Spectroscopic Imaging of Concealed Low-Absorbing Objects. *Opt. Eng.* **2019**, *58*, 023104. [CrossRef]
19. Zdanevičius, J.; Čibiraitė, D.; Ikamas, K.; Bauer, M.; Matukas, J.; Lisauskas, A.; Richter, H.; Hagelschuer, T.; Krozer, V.; Hubers, H.W.; et al. Field-Effect Transistor Based Detectors for Power Monitoring of THz Quantum Cascade Lasers. *IEEE Trans. Terahertz Sci. Technol.* **2018**, *8*, 613–621. [CrossRef]
20. Bauer, M.; Rämer, A.; Chevtchenko, S.A.; Osipov, K.Y.; Čibiraitė, D.; Pralgauskaitė, S.; Ikamas, K.; Lisauskas, A.; Heinrich, W.; Krozer, V.; et al. A high-sensitivity AlGaN/GaN HEMT Terahertz Detector with Integrated Broadband Bow-tie Antenna. *IEEE Trans. Terahertz Sci. Technol.* **2019**, *9*, 430–444. [CrossRef]
21. Ikamas, K.; Čibiraitė, D.; Lisauskas, A.; Bauer, M.; Krozer, V.; Roskos, H.G. Broadband Terahertz Power Detectors Based on 90-Nm Silicon CMOS Transistors with Flat Responsivity up to 2.2 THz. *IEEE Electron. Device Lett.* **2018**, *39*, 1413–1416. [CrossRef]
22. Veksler, D.; Muravjov, A.; Stillman, W.; Pala, N.; Shur, M. Detection and Homodyne Mixing of Terahertz Gas Laser Radiation by Submicron GaAs/AlGaAs FETs. In Proceedings of the SENSORS, 2007 IEEE, Atlanta, GA, USA, 28–31 October 2007; pp. 443–445. [CrossRef]
23. Preu, S.; Kim, S.; Verma, R.; Burke, P.G.; Vinh, N.Q.; Sherwin, M.S.; Gossard, A.C. Terahertz Detection by a Homodyne Field Effect Transistor Multiplicative Mixer. *IEEE Trans. Terahertz Sci. Technol.* **2012**, *2*, 278–283. [CrossRef]
24. Preu, S.; Regensburger, S.; Kim, S.; Mittendorff, M.; Winnerl, S.; Malzer, S.; Lu, H.; Burke, P.G.; Gossard, A.C.; Weber, H.B.; et al. Broadband THz detection and homodyne mixing using GaAs high-electron-mobility transistor rectifiers. In *Millimetre Wave and Terahertz Sensors and Technology VI*; Salmon, N.A., Jacobs, E.L., Eds.; International Society for Optics and Photonics, SPIE: Bellingham, WA, USA, 2013; Volume 8900, pp. 137–145. [CrossRef]
25. Rumyantsev, S.; Liu, X.; Kachorovskii, V.; Shur, M. Homodyne phase sensitive terahertz spectrometer. *Appl. Phys. Lett.* **2017**, *111*, 121105. [CrossRef]
26. Knap, W.; Dyakonov, M.; Coquillat, D.; Teppe, F.; Dyakonova, N.; Łusakowski, J.; Karpierz, K.; Sakowicz, M.; Valusis, G.; Seliuta, D.; et al. Field Effect Transistors for Terahertz Detection: Physics and First Imaging Applications. *J. Infrared Millimeter Terahertz Waves* **2009**, *30*, 1319–1337. [CrossRef]
27. Dyakonov, M.; Shur, M. Detection, mixing, and frequency multiplication of terahertz radiation by two-dimensional electronic fluid. *IEEE Trans. Electron. Dev.* **1996**, *43*, 380–387. [CrossRef]
28. Lisauskas, A.; Pfeiffer, U.; Öjefors, E.; Haring Bolìvar, P.; Glaab, D.; Roskos, H.G. Rational design of high-responsivity detectors of terahertz radiation based on distributed self-mixing in silicon field-effect transistors. *J. Appl. Phys.* **2009**, *105*, 114511. [CrossRef]
29. Boppel, S.; Ragauskas, M.; Hajo, A.; Bauer, M.; Lisauskas, A.; Chevtchenko, S.; Rämer, A.; Kašalynas, I.; Valušis, G.; Würfl, H.J.; et al. 0.25-um GaN TeraFETs Optimized as THz Power Detectors and Intensity-Gradient Sensors. *IEEE Trans. Terahertz Sci. Technol.* **2016**, *6*, 348–350. [CrossRef]
30. Bauer, M.; Rämer, A.; Boppel, S.; Chevtchenko, S.; Lisauskas, A.; Heinrich, W.; Krozer, V.; Roskos, H.G. High-sensitivity wideband THz detectors based on GaN HEMTs with integrated bow-tie antennas. In Proceedings of the 10th European Microwave Integrated Circuits Conference (EuMIC), Paris, France, 7–8 September 2015; pp. 1–4. [CrossRef]

31. Nellen, S.; Ishibashi, T.; Deninger, A.; Kohlhaas, R.B.; Liebermeister, L.; Schell, M.; Globisch, B. Experimental Comparison of UTC- and PIN-Photodiodes for Continuous-Wave Terahertz Generation. *J. Infrared Millimeter Terahertz Waves* **2020**, *41*, 343–354. [CrossRef]
32. Müller, R.; Bohmeyer, W.; Kehrt, M.; Lange, K.; Monte, C.; Steiger, A. Novel detectors for traceable THz power measurements. *J. Infrared Millimeter Terahertz Waves* **2014**, *35*, 659–670. [CrossRef]
33. But, D.B.; Drexler, C.; Sakhno, M.V.; Dyakonova, N.; Drachenko, O.; Sizov, F.F.; Gutin, A.; Ganichev, S.D.; Knap, W. Nonlinear photoresponse of field effect transistors terahertz detectors at high irradiation intensities. *J. Appl. Phys.* **2014**, *115*, 164514. [CrossRef]
34. Rudin, S.; Rupper, G.; Shur, M. Ultimate response time of high electron mobility transistors. *J. Appl. Phys.* **2015**, *117*, 174502. [CrossRef]
35. Sun, J.D.; Sun, Y.F.; Wu, D.M.; Cai, Y.; Qin, H.; Zhang, B.S. High-responsivity, low-noise, room-temperature, self-mixing terahertz detector realized using floating antennas on a GaN-based field-effect transistor. *Appl. Phys. Lett.* **2012**, *100*, 013506. [CrossRef]
36. Čibiraitė, D.; Bauer, M.; Lisauskas, A.; Krozer, V.; Roskos, H.G.; Ramer, A.; Krozer, V.; Heinrich, W.; Pralgauskaite, S.; Zdanevicius, J.; et al. Thermal Noise-Limited Sensitivity of FET-Based Terahertz Detectors. In Proceedings of the 2017 International Conference on Noise and Fluctuations (ICNF), Vilnius, Lithuania, 20–23 June 2017; pp. 1–4. [CrossRef]
37. Qin, H.; Li, X.; Sun, J.; Zhang, Z.; Sun, Y.; Yu, Y.; Li, X.; Luo, M. Detection of incoherent terahertz light using antenna-coupled high-electron-mobility field-effect transistors. *Appl. Phys. Lett.* **2017**, *110*, 171109. [CrossRef]
38. Čibiraitė-Lukenskienė, D.; Ikamas, K.; Lisauskas, T.; Krozer, V.; Roskos, H.G.; Lisauskas, A. Passive Detection and Imaging of Human Body Radiation Using an Uncooled Field-Effect Transistor-Based THz Detector. *Sensors* **2020**, *20*, 4087. [CrossRef] [PubMed]
39. Yahyapour, M.; Vieweg, N.; Roggenbuck, A.; Rettich, F.; Cojocari, O.; Deninger, A. A Flexible Phase-Insensitive System for Broadband CW-Terahertz Spectroscopy and Imaging. *IEEE Trans. Terahertz Sci. Technol.* **2016**, *6*, 670–673. [CrossRef]